ACSNANO www.acsnano.org

ARTICLE

Self-Recovery Superhydrophobic Surfaces: Modular Design

Emanuele Lisi, Matteo Amabili, Simone Meloni,* Alberto Giacomello,* and Carlo Massimo Casciola

Dipartimento di Ingegneria Meccanica e Aerospaziale, Università di Roma "La Sapienza", Rome, Italy

Supporting Information

ABSTRACT: Superhydrophobicity, the enhanced hydrophobicity of surfaces decorated with textures of suitable size, is associated with a layer of gas trapped within surface roughness. The reduced liquid/solid contact makes superhydrophobicity attractive for many technological applications. This gas layer, however, can break down with the liquid completely wetting the surface. Experiments have shown that the recovery of the "suspended" superhydrophobic state from the wet one is difficult. Self-recovery—the spontaneous restoring of the gas layer at ambient conditions—is one of the dreams of research in superhydrophobicity as it would allow to overcome the fragility of superhydrophobicity. In this work we have performed a theoretical investigation of the wetting and recovery processes on a set of surfaces characterized by textures of different dimensions and morphology in order to elucidate the optimal parameters for avoiding wetting and achieving self-recovery. Results show that texture size in the nanometer range is a necessary condition for self-recovery, but not a sufficient one, the geometry plays a crucial role, and nanopillars prevent self-recovery, while surfaces with square pores exhibit self-recovery even at large positive pressures. However, the optimal morphology for self-recovery, the square pore, is suboptimal for the functional properties of the surface, for example, high slippage. Our calculations show that these properties are related to regions of the texture separated in space: self-recovery is controlled by the characteristics of the bottom surface, while wetting and slip are controlled by the cavity mouth. We thus propose a modular design strategy which combines self-recovery and good functional properties: Square pores surmounted by ridges achieve self-recovery even at 2 MPa and have a very small liquid/solid contact area. The macroscopic calculations, which allowed us to efficiently devise design criteria, have been validated by atomistic simulations, with the optimal texture showing self-recovery on atomic time scales, $\tau \sim 2$ ns.

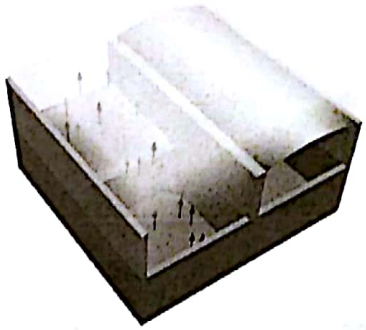

KEYWORDS: *superhydrophobicity, wetting, self-recovery, free energy simulations, sharp interface model, molecular dynamics*

Superhydrophobic surfaces are textured surfaces made of hydrophobic materials. A liquid in contact with such surfaces can be suspended over a gas layer entrapped in the cavities by capillary forces: the Cassie–Baxter state[1] (CB, Figure 1a). The reduced contact area with the solid makes the superhydrophobic Cassie–Baxter state suitable for self-cleaning,[2,3] anti-icing,[4−6] humidity-proof coatings,[7,8] micro-condensation,[9] drag reduction,[10−12] oil–water separation,[13−15] superhydrophobic electrodes for batteries and fuel cells,[16−18] prevention of corrosion,[19,20] and other technological applications. On the same surface and under the same conditions, a liquid might also completely wet the textures. In this case the system is said to be in the Wenzel state[21] (W, Figure 1b), which is characterized by very large liquid/solid contact area. The superhydrophobic properties of textured surfaces are related to the intervening gas layer (Cassie–Baxter state). For this reason, one should speak of superhydrophobic states rather than superhydrophobic surfaces.

In typical applications, Cassie–Baxter and Wenzel are two stable or metastable states of the system. A surface prepared in the metastable state (*e.g.*, Cassie–Baxter) can remain in the initial configuration for long time scales, which depends on the thermodynamic conditions and on the texture characteristics. It is clear that in most applications the transition from the Cassie–Baxter to the Wenzel state should be delayed or avoided. At the same time, it is desirable to favor the reverse transition from the Wenzel to the Cassie–Baxter state—the recovery of superhydrophobicity—should the system undergo wetting due, for example, to a temporary change of external conditions. The aim of the present work is to design the geometry and morphology of surface textures in order to realize surfaces that cannot be wetted under normal conditions, and even when this happens, they are capable of rapidly recovering without external inputs.

An experiment in which the pressure is increased from ambient conditions and subsequently restored can help to

Received: September 10, 2017
Accepted: November 28, 2017
Published: November 28, 2017

DOI: 10.1021/acsnano.7b06438
ACS Nano XXXX, XXX, XXX−XXX

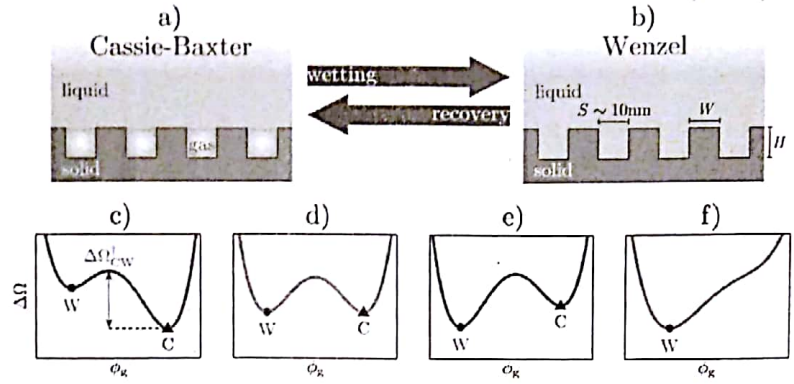

Figure 1. Cartoon illustrating the configuration of the Cassie–Baxter (a) and Wenzel (b) states, the metastable states of a system consisting of a liquid (l) and gas (g) in contact with a solid surface (s) with (simple) textures. In the panel (b) are illustrated the characteristic dimensions of the surface textures considered in the present work: the thickness W, the spacing (pitch) S, and the height H. (c–f) Cartoon of energy profiles along the wetting/recovery process at various pressures (pressure increases in going from panels c to f). At low pressure (c) Cassie–Baxter is stable and Wenzel is metastable. Increasing the pressure, the heterogeneous coexistence is achieved (d) at which the two states (minima) have the same free energy. Further increasing the pressure, Wenzel becomes the stable state (e), but the two states are still separated by a large barrier, much higher than the thermal energy. Finally, at large pressures, there is no minimum in correspondence of the Cassie–Baxter state: Wenzel is the only stable state available to the system.

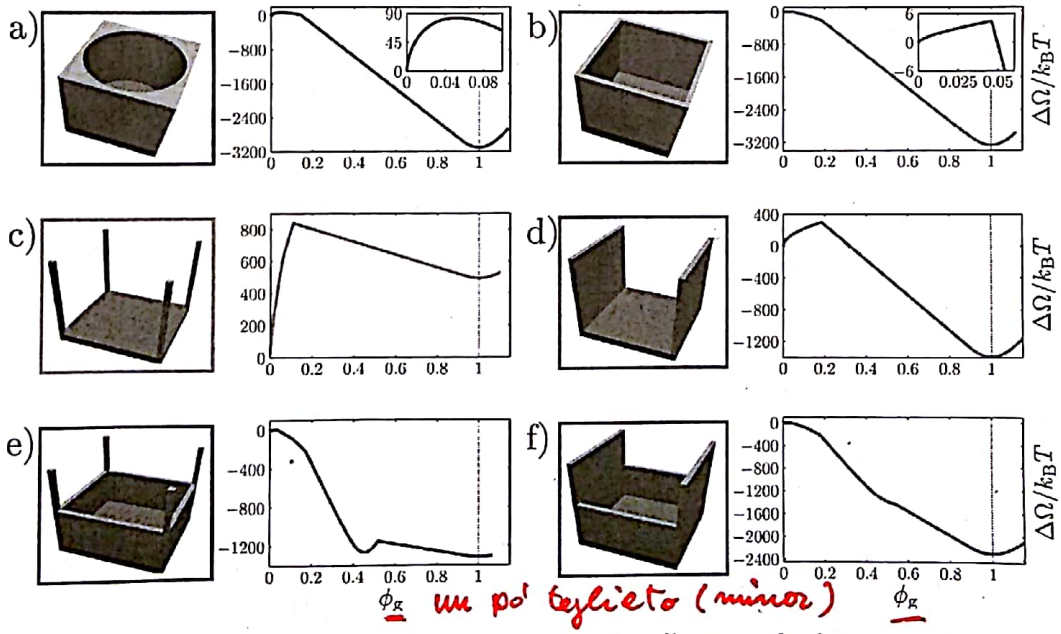

Figure 2. Surface textures considered in this work together with grand-potential profiles expressed in k_BT units as a function of gas volume fraction (ϕ_g) in the cavities at ambient conditions ($\Delta P \approx 0.1$ MPa). (a) Circular and (b) square pores, (c) pillars, and (d) ridges. The final panels show the proposed modular textures: (e) square pores/pillars and (f) square pores/ridges.

understand the problem of wetting and recovery in more rigorous terms, following the equilibrium arguments of, for example, refs 22 and 23. At ambient conditions the free energy of the system presents two minima (Figure 1c): an absolute minimum (the stable state, Cassie–Baxter in the hypothesis) and a local minimum (the metastable Wenzel state) separated by a free-energy barrier $\Delta\Omega^{\dagger}_{CW}$. Thus, if this specific system is initially prepared in the Cassie–Baxter state, then it remains in this state. When the pressure increases, the difference of free energy $\Delta\Omega_{CW} = \Omega_C - \Omega_W$ between the Cassie–Baxter and Wenzel states increases from negative values. Eventually, $\Delta\Omega_{CW}$ becomes zero at the heterogeneous coexistence pressure P^{co} (Figure 1d) and positive for $P > P^{co}$ (Figure 1e). At moderate pressures the barrier separating the Cassie–Baxter and Wenzel states, $\Delta\Omega^{\dagger}_{CW}$, is much larger than the thermal energy available to the system, k_BT, where k_B is the Boltzmann constant and T the temperature. Thus, the transition time $\tau = \tau_0 \exp(\Delta\Omega^{\dagger}_{CW}/k_BT)$[24,25] is longer than the experimental time of observation. Therefore, the system remains kinetically trapped in the Cassie–Baxter state even when this is metastable. Upon additional increase of the pressure, the barrier decreases until it becomes small enough that the system can readily undergo the Cassie–Baxter/Wenzel transition (Figure 1f). If the initial external conditions are restored, the recovery barrier $\Delta\Omega^{\dagger}_{WC}$ is very large, the system remains kinetically trapped in the Wenzel state (Figure 1b), and recovery cannot be achieved. This

DOI: 10.1021/acsnano.7b06438
ACS Nano XXXX, XXX, XXX–XXX

experiment illustrates why several experimental and theoretical works[22,23,26] report that the Cassie–Baxter/Wenzel transition is irreversible for standard surfaces operating near ambient conditions.

Several strategies have been developed to preserve[27−30] or recover[31−33] the Cassie–Baxter state. Hierarchical surfaces have been fabricated to increase the intrusion pressure, but no quantitative design criteria have been identified yet to fabricate optimal systems. *Active* approaches to enhance wetting resistance have also been considered, such as pressurization of the gas layer,[28,29] but this adds complexity to the system. Concerning the recovery, several strategies have been developed, including the *in situ* development (and spread) of gas,[31] electrical switching,[32,34] mechanical vibration,[33] but these approaches add complexity to the system.

Ideally, a superhydrophobic surface should be able to withstand the highest possible pressure without undergoing a wetting transition[22,23,35−41] and recover the Cassie–Baxter state once the perturbation has ceased (self-recovery). Pioneering attempts to design surfaces with these characteristics were based on heuristic hypotheses on the Cassie–Baxter/Wenzel transition mechanism.[42−46] More recently, Prakash *et al.*[47] have proposed the modification of the internal part of nanopillar surfaces by a sphere of hydrophobic material to enhance the resistance to the wetting and promote the recovery. A possible drawback of this approach is that the hydrophobic sphere necessary to make the recovery barrier negligible occupies most of the surface cavities, which might affect the function of the surface. Giacomello *et al.*[48] have shown that self-recovery can be achieved even at large pressures, if the surface textures have the characteristic size of 2 nm or less; the precise dimension depends on the contact angle of the surface. Here, building upon these early attempts we identify design principles of self-recovery surfaces which do not affect their functional properties.

To achieve our objectives, we first consider a number of surfaces with textures of technological interest and investigate their properties with respect to liquid intrusion and extrusion. In particular, we focus on surfaces decorated with circular and square pores, square pillars, and ridges of nanoscopic size (Figure 2a–d). We investigate the dependence on the liquid pressure of the wetting and recovery barriers for these systems. From this analysis one identifies the fundamental design principles affecting the resistance to wetting and self-recovery abilities. Second, on the basis of the wetting properties of simple texture morphologies, we design surfaces combining good superhydrophobic characteristics, robustness of the Cassie–Baxter state, and self-recovery properties (Figure 2e,f). For our best surface, we also identify the maximum possible size of the texture that still allows self-recovery, which is a key fabrication parameter.

The present analysis is based on a combined macro- and microscopic approach. The wetting and recovery mechanism and barrier of the extended set of systems is studied by the continuum rare events method (CREaM),[36] which identifies transition barriers for a liquid in a complex confining environment based on the sharp interface model of a solid–liquid–gas system. For selected systems, results are validated by *standard* molecular dynamics (MD) and by restrained molecular dynamics (RMD),[49,50] a simulation technique designed to compute the free-energy profile of systems characterized by large free-energy barriers.

Anticipating our results, we show that the recovery barrier is essentially determined by the morphology and geometrical characteristics of the bottom of the corrugations, while the wetting barrier is mainly associated with the characteristics of the top part of the textures. It turns out that the most efficient topography for self-recovery is the surface with square nanopores, which, however, typically has a large liquid/solid contact area, resulting in unsatisfactory superhydrophobic properties. Moreover, in square-pore surfaces, one of the walls of the textures is orthogonal to the flow, with potential limitations to the drag reduction. Pillar and ridge surfaces, on the contrary, present lower liquid/solid contact areas and perform better at reducing drag,[51] but their recovery barrier is very large making the wetting process typically irreversible. These observations brought us to propose a modular design of textured surfaces consisting of the combination of simple texture morphologies of the kinds listed above. In particular, we have found that the combination of ridges and square pores, resulting in a topography of ridge textures with transversal bulkheads at their bottom, renders surfaces highly resistant to wetting, capable of self-recovery, and retaining the good superhydrophobic properties of ridges.

RESULTS AND DISCUSSION

We study the thermodynamics and kinetics of the wetting and recovery by considering the grand potential Ω of the system as a function of the volume of gas V_g in the surface corrugations. This grand potential profile is obtained from a macroscopic model of the three-phase solid–liquid–gas system as explained in the Methods section. From the grand potential profile (Figure 1c–e) one obtains the wetting $\Delta\Omega^{\dagger}_{CW}$ and recovery $\Delta\Omega^{\dagger}_{WC}$ barriers at different pressures. In the present work we take as the operative definition of intrusion pressure, P^{int} (extrusion pressure, P^{ext}), the pressure at which the wetting (recovery) barrier is $25k_BT$, corresponding to a transition time $\tau = \tau_0 \exp(\Delta\Omega^{\dagger}/k_BT) = 1$ s,[25] that is, the order of magnitude of the typical experimental time. From Ω one obtains also the coexistence pressure P^{co} for the heterogeneous system, that is, the pressure at which the Cassie–Baxter and Wenzel states have the same grand potential (Figure 1d).

The three-phase system is described in terms of the sharp interface model, consisting of solid, liquid, and gas bulk domains separated by sharp discontinuities at their interfaces. The corresponding grand potential is the sum of bulk and interface terms: $\Omega = -P_sV_s - P_lV_l - P_gV_g + \gamma_{sl}A_{sl} + \gamma_{lg}A_{lg} + \gamma_{sg}A_{sg}$, where P_x and V_x are the pressure and volume of a generic phase x and γ_{xy} and A_{xy} are the surface tension and area between the x and y phases, respectively. Considering that the solid surface does not change during the process, the state of the system is fully characterized by the liquid/gas interface— the meniscus—whose intersection with the solid surface determines the volume of each phase and the areas of the various interfaces. The (relative) grand potential can be recast into the more convenient form:

$$\Delta\Omega = \Delta P V_g + \gamma_{lg}(A_{lg} + \cos\theta_Y A_{sg}) \quad (1)$$

where the Young contact angle $\cos\theta_Y = (\gamma_{sg} - \gamma_{sl})/\gamma_{lg}$ depends on the chemical nature of the solid, liquid, and gas and $\Delta P = P_l - P_g$ is the difference between the pressure of the liquid and the gas. Within the sharp interface approximation, in which surface tension terms do not depend on the pressure, for a given surface morphology and chemistry, ΔP determines the relative

DOI: 10.1021/acsnano.7b06438
ACS Nano XXXX, XXX, XXX−XXX

stability of the Cassie–Baxter and Wenzel states. For convenience, in the following we will report Ω as a function the gas volume fraction $\phi_g = V_g/V_T$, where V_T is the volume of the texture cavities.

The wetting and recovery processes can proceed with the liquid entering into or exiting from the textures along different trajectories. By trajectory we mean the sequence of meniscus configurations along the wetting/recovery, that is, as a function of ϕ_g. Different paths are characterized by different grand potential profiles which correspond to different meniscus morphologies along the process and, thus, to different values of the interface terms in eq 1. Among these trajectories, we consider that of maximum probability as identified by the continuum rare event method (CREaM – described in the Methods section), and along it we compute Ω (see Supporting Information for a discussion on wetting *via* the depinning *vs* sagging mechanisms). θ_Y is set to 125°, corresponding to the *state of the art* hydrophobic materials,[52,53] and γ_{lg} = 0.072 N/m, that is, the surface tension of water at room temperature.

We first consider the wetting/recovery characteristics of four basic types of textures of interest for technological applications: (i) circular and (ii) square pores, (iii) pillars, and (iv) ridges (Figure 2a–d). The geometry of these textures is characterized by three parameters: the spacing (S), the thickness (W), and the height (H) of the solid part of the corrugations (Figure 1b). The detailed study of how these three geometrical parameters affect the relative stability of the Cassie–Baxter *vs* Wenzel state, the wetting and recovery barriers, the intrusion and extrusion pressure, and their dependence on the temperature will be discussed in a forthcoming article. Here we focus on the analysis and design of textures in a range allowing for self-recovery. In particular, we consider textures of thickness W = 1 nm, with S and H chosen such that the cross section and volume of the texture are 121 nm^2 and 1100 nm^3, respectively ($S \sim H \sim 10$ nm). As we will discuss more in detail below, this size is in the range allowing self-recovery at ambient conditions.

In Figure 2a–d we report the grand potential as a function of the amount of gas in the cavities at ambient conditions. The shape of these curves is qualitatively similar, with two minima corresponding to the Cassie–Baxter and Wenzel states separated by a barrier. For all but the pillar system, the grand potential of the Cassie–Baxter state is lower than the Wenzel one, that is, Cassie–Baxter is stable and Wenzel is metastable. For the pillars the order of stability between the two wetting states is opposite because of the small hydrophobic surface area of the thin structures considered in the present work; thicker pillars (higher W) or a smaller pitch (lower S) will eventually result in a stabilization of the Cassie–Baxter over Wenzel state. Nevertheless, even when the Cassie–Baxter state is metastable, due to the large wetting barrier and the correspondingly long transition time (Table 2), a droplet deposited on the pillar surface or the surface immersed in a liquid will remain in the superhydrophobic state for experimentally relevant times.

We remark that all the systems considered have a high intrusion pressure due to their reduced size; among those, the pore surfaces, in particular the square pore, can better resist to intrusion. The superior ability of pore surface to resist to intrusion can be intuitively understood considering that the driving force of the wetting, $\Delta P V_g$, which is the same for all systems, is opposed by the solid/liquid–solid/gas surface term, $\gamma_{lg} \cos\theta_Y A_{sg}$, which is maximum in the square pore case.

Upon large pressure variations such that $P \geq P^{int}$, caused, for example, by impact[54] or evaporation[37] of a water droplet, or by turbulence in submerged applications,[55] the system readily undergoes a Cassie–Baxter/Wenzel transition. Experiments show that typically when the external perturbation triggering the transition terminates, for example, if the pressure perturbation decreases, the system remains in the Wenzel state, that is, the transition is irreversible.[22] The reason is that in the original conditions, typically ambient pressure and temperature, the recovery barrier is very large. This is the case of the nanoscopic pillar and ridge surfaces considered in this work (Figure 2c,d), which at ambient conditions present recovery barriers of 840 and 309 k_BT, respectively, corresponding to recovery times $\tau_{WC} \sim 10^{355}$ and $\tau_{WC} \sim 10^{123}$ s (Table 2). The recovery barrier is much lower in the case of circular and square pores. In particular, in the case of the square pore the recovery barrier at ambient conditions is $\Delta\Omega^{\dagger}_{WC}$ = 5.7 k_BT and recovery time $\tau_{WC} = 3 \times 10^{-9}$ s. In other words, nanoscale square-pore surfaces are capable of self-recovery at ambient conditions. Actually, our calculations show that nanoscopic square pore surfaces are capable of self-recovery also at positive pressures, up to $P^{ext} \sim 1.8$ MPa (Table 1). The extrusion pressures of the four systems follows the ordering *square pore* > *circular pore* > *ridges* > *pillars* (Table 1). In particular square pores are the only system with a positive P^{ext}. These results show that nanocorrugations are necessary but not sufficient for self-recovery. The morphology of textures crucially affects the recovery barrier and extrusion pressure.

The relation between $\Delta\Omega^{\dagger}_{WC}$, P^{ext}, and the morphology of the textures can be understood noticing that the configuration of the system at the transition state—the maximum of the grand potential—is a gas bubble at the intersection between the solid part of the textures and the bottom wall (Figure 2). The gas bubble is formed at this place because here the highest ratio $\chi = A_{sg}/A_{lg}$ is achieved. According to the sharp interface model of eq 1, the denominator is associated with the energy penalty of

Table 1. Characteristics of the Textured Surfaces Considered in the Present Work[a]

	P^{co} (MPa)	$\Delta\Omega^{\dagger}$ (k_BT)	P^{int} (MPa)	P^{ext} (MPa)	f	θ (°)
circular pore	12.6	476	14.9	−9.4	0.24	154
square pore	13.9	421	16.4	1.8	0.17	158
pillars	−1.6	788	1.3	−52.7	0.01	175
ridges	5.4	568	8.1	−17.8	0.09	164
square pore/ pillars	11.0	283	15.7	−7.14	0.01	175
square pore/ ridges	11.1	289	15.7	2.0	0.09	164

[a] P^{co} is the heterogeneous coexistence pressure, and $\Delta\Omega^{\dagger}$ is the corresponding wetting and recovery barrier. For the modular structures (pore/pillars and pore/ridges), P^{co} is the coexistence pressure between the Wenzel and the *intermediate* Cassie–Baxter (iC) state. There is no pressure at which Wenzel and Cassie–Baxter have the same Ω for these surfaces. P^{int} and P^{ext} are the intrusion and extrusion pressures at room temperature, respectively. As explained in the text, the operative definition of intrusion and extrusion pressure is the pressure at which the corresponding barrier is 25 k_BT. For modular structures, in which the system presents three metastable states, P^{int} and P^{ext} are determined by the largest of the two iC/C and iC/W barriers. In particular, for both modular surfaces, the intrusion pressure is the one at which $\Delta\Omega^{\dagger}_{iCW}$ = 25 k_BT. Concerning the extrusion pressure, the relevant barrier is $\Delta\Omega^{\dagger}_{iCC}$ for the square pore/pillar surface and $\Delta\Omega^{\dagger}_{WiC}$ for the square pore/ridge one. The solid fraction f and the corresponding apparent contact angle θ for a system in the Cassie–Baxter state are also reported.

DOI: 10.1021/acsnano.7b06438
ACS Nano XXXX, XXX, XXX–XXX

Table 2. Wetting and Recovery Characteristics of *Standard* and Modular Surfaces at Ambient Conditions[a]

	$\Delta\Omega^{\dagger}_{CW}$ (k_BT)	τ_{CW} (s)	$\Delta\Omega^{\dagger}_{WC}$ (k_BT)	τ_{WC} (s)
circular pore	3169	2×10^{1365}	84	5×10^{25}
square pore	3254	1×10^{1402}	5.7	3×10^{-9}
pillars	320	1×10^{128}	843	2×10^{355}
ridges	1671	6×10^{714}	309	1×10^{123}
square pore/pillars	152.5/1257	$2 \times 10^{55}/3 \times 10^{534}$	6.5/115.5	$7 \times 10^{-9}/1 \times 10^{39}$
square pore/ridges	2274	6×10^{976}	6.3	6×10^{-9}

[a]wetting, $\Delta\Omega^{\dagger}_{CW}$, and recovery, $\Delta\Omega^{\dagger}_{WC}$, barriers and corresponding times, τ_{CW} and τ_{WC}. At ambient conditions the modular square pore/pillars surface has three metastable states. Thus, the overall wetting and recovery processes are characterized by two barriers each and the associated transition times, corresponding to the C → iC and iC → W (left and right numbers of the slash), and W → iC and iC → C, respectively.

forming a liquid/gas interface, $\gamma_{lg}A_{lg}$, and the numerator to the energy gain of heterogeneous nucleation at an hydrophobic surface, $\gamma_{lw}\cos\theta_Y A_{sg}$, ($\cos\theta_Y < 0$ for hydrophobic surfaces); the value of this ratio is maximum for a bubble located at the intersection between the vertical and the bottom walls of the cavity, which is where nucleation takes place. In addition, for a bubble of prescribed volume, for example, the volume of the critical bubble of the square pore, this ratio is higher in the square pore ($\chi = 1.73$), followed by the circular pore ($\chi = 1.46$), the ridge ($\chi = 1.41$) and, finally, the pillars ($\chi = 0.97$).

To summarize, all the nanotextured surfaces analyzed here are able to resist to intrusion under the action of intense pressures, with $P^{int} \in [1.28, 16.37]$ MPa, and the pore surface emerges as the best one at resisting intrusion and at achieving recovery, with those decorated with square pores being able to self-recover at positive pressures.

One might be tempted to consider the square pore surface optimal for superhydrophobic applications. However, it must be remarked that for a prescribed thickness W, pore surfaces have a much higher solid fraction f (Table 1)—the ratio between the solid surface wet by the liquid in the Cassie–Baxter state A_{wet} over the nominal surface $A_{nominal}$—which might affect their *functional* properties. For example, the apparent contact angle θ is an important parameter to characterize emerged applications of superhydrophobicity, that is, those involving a rough surface immersed in air and in contact with liquid drops. Typically, the higher the θ, the better the surface is at repelling drops. In the Cassie–Baxter state the apparent contact angle is given by[1] $\cos\theta = f(\cos\theta_Y + 1) - 1$, where f is the solid fraction. Thus, for a given surface chemistry, encoded by θ_Y, the emerged superhydrophobicity, θ, increases with decreasing solid fraction. The apparent contact angle of the four surfaces considered here is $\theta_{circular} = 154°$, $\theta_{square} = 158°$, $\theta_{ridges} = 164°$, and $\theta_{pillars} = 175°$. A quantitative comparison for the effect of morphology on drag is more complex, but experimental and theoretical works have shown that pillars and ridge surfaces are better suited for these applications than the others considered here. For instance, ref 51 numerically investigates the case of laminar flows, predicting slip lengths of 30 nm for pillars, 7 nm for ridges, and 2 nm for square pores with the same f as the present work. For turbulent flows, ridges perform best among the investigated textures.[10] Our results suggest that a single elementary texture is unable to satisfy all the requirements of superhydrophobic surfaces: resistance to wetting, self-recovery, high contact angle, and/or low drag, *etc.*

Here we propose a modular design for achieving optimal characteristics for emerged and submerged applications of superhydrophobic surfaces. This approach consists of combining two texture morphologies with the same characteristic length on the same surface: a square pore combined with pillars or with ridges (Figure 2e,f). This approach is inspired by the observation that the regions of the textures responsible for the recovery and for the functional properties of the surface are separated in space. Recovery is determined by the morphology and geometry of the bottom, while functional properties are controlled by the characteristics of the top of corrugations, that is, by the cavity mouth. In particular, since the recovery transition state consists of a small bubble at one of the bottom corners of the pore ($\phi_g = 0.046$, Figure 2b), a shallow pore is sufficient to induce self-recovery. Thus, the idea is to install pillars or ridges on top of the pore to obtain a modular surface with, at the same time, optimal functional and recovery properties. The two modular surfaces we consider have the same overall height of the pillar and ridge surfaces, with the bottom half consisting of the square pore and the top half of pillars or ridges.

In the modular surfaces one might observe the formation of an additional metastable state that we denote as *intermediate* Cassie–Baxter (iC). This state corresponds to a configuration in which the meniscus is pinned at the top of the square pore, see Figure SI4 in the Supporting Information. Thus, depending on the pressure, with modular surfaces the system might have to overcome two barriers, W → iC and iC → C, during the recovery process. The largest of the two barriers determines the recovery time. The dependence of the two barriers on the pressure might be different, and for both modular surfaces, the intrusion pressure is determined by the WiC barrier. Concerning the extrusion pressure, the relevant barrier is $\Delta\Omega^{\dagger}_{iCC}$ for the square pore/pillar surface and $\Delta\Omega^{\dagger}_{WiC}$ for the square pore/ridge one.

As expected, the square pore/pillar surface (Figure 2e) presents a low W → iC barrier, below 6.5 k_BT ($\phi_g = 0.03$), with a corresponding transition time of 7 ns (Table 2). However, at ambient conditions the intermediate Cassie–Baxter state is separated from the true Cassie–Baxter state by a barrier of 115.45 k_BT, much lower than the single barrier of the system with only pillars, but still corresponding to the very large recovery times $\tau \sim 10^{39}$ s. This means that along the process the meniscus remains trapped at the intermediate Cassie–Baxter state and recovery takes place only at very negative pressures, $P^{ext} = -7.1$ MPa. However, at these pressures the true Cassie–Baxter state is neither stable nor metastable and the system evaporates. (The Cassie–Baxter state for the pillar surface considered in this work is metastable with respect to evaporation only up to ~−1 MPa.)

The iC → C barrier is associated with the depinning of the meniscus from the center of the edges of the pore. This suggests that reducing the number of edges, for example, by combining the square pore with ridges, one could obtain a self-

DOI: 10.1021/acsnano.7b06438
ACS Nano XXXX, XXX, XXX−XXX

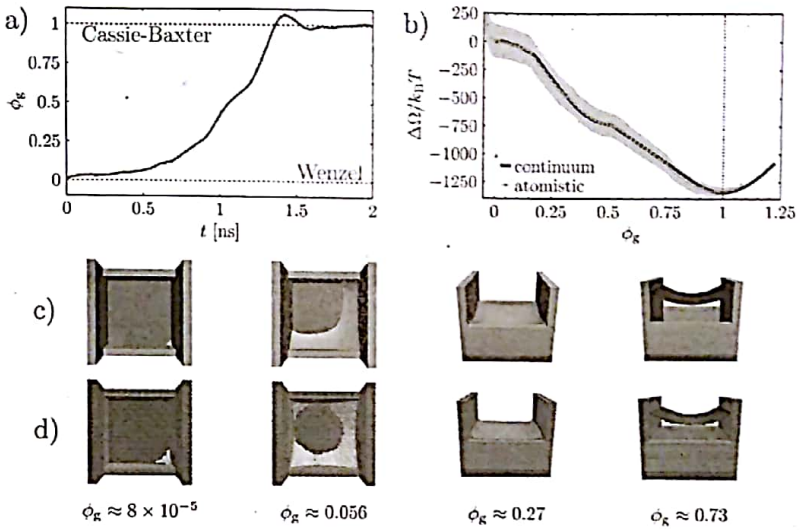

Figure 3. (a) Gas volume fraction as a function of time along a MD starting from the Wenzel state at ambient conditions for the square pore/ridge surface. Complete recovery is achieved within 1.5 ns. (b) Comparison between the atomistic and continuum grand potential; continuum data has been obtained without any fitting of atomistic results. The gray area represents the confidence interval associated with the determination of the atomistic Ω profile. (c and d) Selected meniscus configurations observed along recovery in continuum and atomistic simulations, respectively, at corresponding ϕ_g values.

recovery surface without intermediate states (Figure 2f). As expected, the modular square-pore/ridge surface presents no major differences from the square-pore/pillar and square-pore ones in the first part of the grand canonical potential profile, when the meniscus is within the pore. However, at variance with the square-pore/pillar surface, the barrier between the internal and external Cassie–Baxter states is negligible at ambient conditions, and the system is capable of full self-recovery. It is worth remarking that the for square-pore/ridge, the intermediate Cassie–Baxter state exists only at pressures greater than ca. 3.5 MPa.

In summary, the modular square-pore/ridge surface combines self-recovery properties characterized by positive extrusion pressure (P^{ext} = 2.0 MPa, associated with the W → iC step of the path) to good functional properties, for example, an apparent contact angle of θ = 164°. Further analysis shows that textured surfaces of this morphology can achieve self-recovery at ambient conditions up to a characteristic length of $S \sim 20$ nm (see Figure SI5). This size is typically smaller than the one achievable for the fabrication of complex textures by *top down* approaches, such as standard photolithography.[56−58] To go beyond this limitation, in the future we plan to study textures of simpler fabrication based on the modular principles established in this work. Nevertheless, larger modular textures, within the range accessible by standard photolitography,[59] enhance and facilitate the recovery with active approaches (see Figure SI7). It must be remarked that specialized techniques have been recently introduced[60,61] which are very promising for the fabrication of nanoscopic textured surfaces in the range investigated in the present work (10–20 nm) and might be used to implement the ~~modular~~ design proposed here.

Comparison with Molecular Dynamics. The sharp interface model adopted for modeling the continuum multi-phase system implies a number of approximations which might affect the value of the wetting and recovery barriers, especially at the nanoscale. Thus, to validate the results discussed above, we have performed atomistic simulations of the recovery of the modular square-pore/ridge surface. The atomistic square-pore/ridge surface, shown in Figure SI2, is obtained from a face-centered cubic crystal of Lennard-Jones (LJ) particles with a 0.36 nm lattice parameter. The solid particles interact with the oxygen atoms of the water molecules by a modified LJ potential, which allowed us to tune the Young contact angle of the material to the same value used in the continuum calculations. More details are given in the Methods section. The atomistic texture pitch, thickness, and height are S = 29 atoms, W = 6 atoms, and H = 25 atoms, of which 11 are relative to the pore. These correspond to slightly different values ~~to~~ from those used in the previous section, namely S = 10 nm, W = 2 nm, and H = 9 nm, of which 4 nm are relative to the pore and 5 nm to the ridge. The direct comparison of atomistic results with continuum calculations in Figure 3 has been performed using these latter values.

We prepared the system in the Wenzel state (Figure 3a) and ran a constant pressure and temperature simulation at ambient conditions (further details in the Methods section). Soon after the beginning of the simulation the gas fraction ϕ_g in the corrugation increases to values corresponding to the formation of a supercritical bubble, indicating the presence of a negligible recovery barrier, of the order of the thermal energy of the system, k_BT. The recovery accelerates during the process ($\dot{\phi}_g > 0$) and, in agreement with continuum predictions, the system does not remain pinned at the internal Cassie–Baxter state. Finally, when the meniscus reaches the top of the ridges, ϕ_g shows damped oscillations resulting from the combined effect of inertia of the system, the pinning of the meniscus at the corners of ridges, and the viscosity of liquid.

To explain the recovery dynamics and draw a more direct comparison with the free-energy sharp interface calculations, we computed the *atomistic* free energy profile as a function of the liquid fraction by restrained molecular dynamics (see section Methods for details). Atomistic and sharp interface results are consistent both from the point of view of the recovery mechanism (Figure 3c-d) and of the energetics (Figure 3b).

DOI: 10.1021/acsnano.7b06438
ACS Nano XXXX, XXX, XXX−XXX

For both models the recovery starts with the formation of a gas bubble at a corner of the square pore. The bubble then spreads along the bottom corners of the pore one after the other until it forms a circular bubble with the liquid touching the bottom wall at the center of the pore. The bubble grows further until it detaches from the bottom wall of the textures and the flat meniscus rises along the pore. Once at the top of the pore, the meniscus gets pinned at an intermediate position, but the pinning force is very small and the recovery continues with an almost-flat meniscus moving up along the ridges until full recovery of the Cassie–Baxter state is achieved. Concerning the energetics, atomistic and sharp interface model Ω is in very good agreement (Figure 3b), below the error of atomistic simulations. The atomistic model shows no metastable Wenzel state, that is, there is no barrier between the Wenzel state, ϕ_g = 0, and the (internal or external) Cassie–Baxter one. This is a small difference from the sharp interface model, which predicts a small but nonzero barrier. Indeed, this is consistent with the known limitation of the sharp interface model that cannot produce a (*strict*, *i.e.*, barrierless) spinodal transition, both in bulk, heterogeneous, and confined systems.[62,63] In the present context this does not represent a severe limitation, rather it indicates that the recovery time predicted by our continuum calculations is an upper limit to the actual value. The absence of the Wenzel/Cassie–Baxter barrier makes it possible to have a prompt recovery (in the nanoseconds range) at ambient conditions for a pore/ridge surface of characteristic length S = 10 nm.

Summarizing, thanks to the separation between the region controlling the recovery—the intersection between the vertical features of the corrugation and bottom wall—and the zone determining the functional characteristics of the superhydrophobic surface—the top of corrugations—one can combine different texture morphologies into a modular surface with optimal functional and recovery characteristics. In particular, we have shown that ridges and square pores can be combined to produce self-recovery superhydrophobic surfaces with very high apparent contact angles.

CONCLUSIONS

In this work, we have investigated the wetting and recovery mechanism and energetics of a set of nanoscale textured surfaces with different morphologies. We have found that a nanoscopic size is a necessary but not sufficient condition for the wetting process to be reversible. Indeed, nanopillars and nanoridges cannot achieve self-recovery after being wet, that is, there is no spontaneous recovery at ambient conditions on experimentally relevant time scales. On the contrary, pore structures, especially the one with square cross section, have very little recovery barrier, and the process takes place readily. The reason for this different behavior is related to the area of the hydrophobic solid exposed to the nucleating gas bubble which starts the recovery process. This solid/gas area of the nucleating bubble, which is maximum at the corner of the square pore, is the energetic gain balancing the penalty associated with the formation of a liquid/gas interface characteristic of the nucleus of the new phase.

The optimal morphology for self-recovery, the square pore, is suboptimal for the functional properties of the surface, for example, the contact angle or slippage. Considering that at ambient conditions the critical gas bubble starting the recovery in a square pore is rather small, with a volume of ~45 nm^3, ϕ_g = 0.046, we propose a modular morphology, with a square pore combined with pillars or ridges. The pore/pillar surface presents an intermediate Cassie–Baxter state resulting from the pinning of the meniscus at the top of the pore. On the contrary, the pore/ridge surface does not present this problem, and it is the optimal combination for self-recovery and functional properties. Self-recovery for such surfaces can be achieved for textures of up to 20 nm.

The results discussed above are based on the analysis of a sharp interface model of the three phase solid–liquid–gas system. These results have been validated by atomistic simulations of the pore/ridge system, which shows self-recovery on the atomistic time scale (2 ns). Indeed, the atomistic model of the three-phase system shows a barrier smaller than that predicted by the sharp interface model, suggesting that actual textured surfaces designed on the basis of the principles presented in this article might be more efficient at self-recovery than estimated from our analysis.

METHODS

CREaM. The wetting/recovery path is computed according to the continuum rare-event method (CREaM).[36] The CREaM path is the sequence of liquid/gas interfaces Σ_{lg}, the meniscus, at a set of values of the gas volume in the cavity ϕ_g corresponding to the absolute constrained minimum (present value of ϕ_g) of the grand potential. In practice, CREaM is an extension of the classical nucleation theory (CNT)[64−66] to the case of vapor/liquid transition in a confined system. The numerical minimization of the constrained grand potential is obtained with the Surface Evolver code.[67] The input parameters for the three-phase system of eq 1 are the Young contact angle, θ_Y = 125°, the surface tension of the liquid, γ_{lg} = 0.072 N/m, and the difference between the liquid and gas pressures, which at ambient conditions is $\Delta P \approx 0.1$ MPa. As shown in Figure 3, the morphology of the meniscus changes along the path, reflecting the change of the relative stability among the different bubble configurations as a function of ϕ_g.

Molecular Dynamics Simulations. Molecular dynamics (MD) simulations have been performed using the LAMMPS code.[68] Water molecules in the liquid and vapor phases are represented by the TIP4P/2015 model.[69] Their interaction with the walls is described by the modified Lennard-Jones (LJ) potential $v(r_{ab}) = 4\epsilon[(\sigma/r_{ab})^{12} - c(\sigma/r_{ab})^6]$, where r_{ab} is the distance between the oxygen atom of water molecules and the LJ atoms of the wall, ϵ and σ are the characteristic energy and length of the LJ interaction, respectively, and c is a parameter which is tuned to achieve the desired θ_Y (see Figure SI1). In the present case, c = 0.75, corresponding to θ_Y = 124.8°. The contact angle is measured by an independent MD simulation in which we deposited and relaxed a large (diameter ~6 nm) cylindrical sessile droplet over a flat surface.

The composite solid–liquid–vapor system is obtained by placing a slab of water molecules between a textured and flat surface oriented orthogonal to the z direction. Periodic boundary conditions are applied along the x and y directions. The atoms of the textured surface are kept fixed during the simulation, while the atoms of the flat surface are allowed to move only in the z direction. A constant force is applied to the atoms of the flat surface to keep the liquid at constant 0.1 MPa pressure. The system is kept at constant 300 K by a Nosé–Hoover chains thermostat.[70]

The atomistic Ω is computed by numerical integration of the mean force $d\Omega/d\phi$, which is obtained by restrained MD (RMD).[40,71−73] RMD consists of running simulations guided by an extended potential $v(r) + \kappa/2(\phi_g(r) - \phi_g^*)^2$, where $v(r)$ is the physical potential and $\kappa/2(\phi_g(r) - \phi_g^*)^2$ is the restraining term forcing the system to visit configurations consistent with the condition $\phi_g(r) = \phi_g^*$. Here $\phi_g(r) = (N_W - N(r))/(N_W - N_{CB})$ is the atomistic estimate of the gas fraction in the textures, with $N(r)$ the number of water molecules in the textures at the present configuration r, and N_W and N_{CB} number of molecules when the system is in the Wenzel and Cassie–Baxter state, respectively, and ϕ_g^* is the present target gas fraction. In the limit of

DOI: 10.1021/acsnano.7b06438
ACS Nano XXXX, XXX, XXX−XXX